Bidabadi *et al. J Wireless Com Network (2023) 2023:89*
https://doi.org/10.1186/s13638-023-02296-7

EURASIP Journal on Wireless Communications and Networking

RESEARCH Open Access

Energy efficient resource allocation for re-configurable intelligent surface-assisted wireless networks

Samaneh Bidabadi[1*], Messaoud Ahmed Ouameur[1*], Miloud Bagaa[1*] and Daniel Massicotte[1]

*Correspondence:
samaneh.bidabadi@uqtr.ca;
messaoud.ahmed.ouameur@uqtr.ca;
miloud.bagaa@uqtr.ca

[1] Department of Electrical and Computer Engineering, University of Quebec at Trois-Rivieres, Trois-Rivieres, Canada

Abstract

This paper focuses on energy-efficient resource allocation in reconfigurable intelligent surface (RIS)-assisted multiple-input-single-output (MISO) communication systems. Specifically, it revisits the solution to the energy efficiency (EE) problem using the alternating optimization (AO) approach. In each AO iteration, the RIS phase optimization is achieved using the gradient descent method, which unfortunately does not guarantee convergence. To overcome this limitation, we propose two alternatives: the Wolfe-based gradient-descent (GAW) EE maximization Algorithm and the trust region (TR)-based EE maximization algorithm. Additionally, we use Dinkelbach's algorithm to obtain the optimal transmit power allocation. Our results demonstrate that the proposed methods outperform the existing approach that uses sequential fractional programming (SFP) for phase optimization and the traditional relay-based method.

Keywords: RIS-assisted Network, Power allocation, Energy efficiency, RIS phase design

1 Introduction

Existing cellular generations will not be able to meet the extraordinary performance demands, such as high spectral efficiency (SE) and massive connectivity, brought on by the innovative new applications anticipated for the 2030 era, which will lead to a need for 6G technology [1, 2]. 6G wireless networks are expected to support the connectivity of a huge variety of users and equipment through the dense deployment of multi-antenna base stations (BSs) and access points (APs). Consequently, the energy-efficiency (EE) behavior of 6G is a crucial topic [3–5]. One of the potential solutions for green communication in 6G is the reconfigurable intelligent surface (RIS), a recently emerging hardware technology with increasing potentiality for large energy consumption reductions [3]. In its simple form, an RIS is a meta-surface made up of numerous inexpensive passive antennas that may effectively reflect the electromagnetic waves impinging on it in a controllable way to favorably alter the propagation environment [5].

However, several obstacles, ranging from performance characterization to network optimization, must be overcome for the effective deployment of energy-efficient RIS systems [7]. Optimizing RIS-aided wireless networks involves employing various approaches [6]. Model-based methods, such as alternating optimization (AO), decompose the joint optimization problem into smaller sub-problems. These are usually solved using techniques like successive convex approximation (SCA), fractional programming (FP), and branch-and-bound (BnB) techniques. These model-based algorithms offer the advantage of providing theoretical guarantees and insights into the optimality of their performance. However, they may be limited by the complexity of the problem and the need for full knowledge of the system. On the contrary, heuristic algorithms focus on local optima and offer low-complexity solutions. They provide a pragmatic approach to optimization but may not guarantee optimality or handle complex dynamic environments effectively. On the other hand, machine learning (ML) techniques, such as reinforcement learning (RL) and supervised learning, offer data-driven approaches that can adapt to dynamic wireless environments. ML techniques have the advantage of learning from data and capturing complex patterns and interactions, allowing them to potentially discover more efficient solutions. However, the effectiveness of ML techniques mainly depends on the quality and quantity of training data and the computational resources required for training and inference.

The use of RISs in wireless networks has been examined in some recent papers, including [4, 5, 9–17]. Among them, [4, 5, 15–17], focused on either power minimization or EE maximization in RIS-assisted wireless networks using model-based optimization methods that are briefly described in Table 1. On the other hand, the authors in [18] and [19–21] use heuristic and ML techniques, respectively, to solve the EE maximization problem in RIS-aided communications. The downlink sum-rate maximization of a wireless communication system with RIS assistance was examined in [9]. By jointly optimizing the transmit beamforming of the AP and the continuous phase shift of RIS's element, a joint beamforming problem is developed in [10] to maximize the received signal power at the user in RIS-assisted multiple input single output (MISO) system. The authors in [11] studied the RIS-enhanced MISO orthogonal frequency division multiplexing (OFDM) downlink system, whereby the RIS's passive beamforming and the BS's transmit power allocation is jointly optimized using the AO framework for increasing the downlink attainable rate. In [12], the use of several RISs to support mm-Wave MISO communications has been studied. The received signal power is maximized by jointly optimizing active and passive beamforming vectors. Meanwhile, the authors in [13] have suggested an element grouping approach of RIS elements, and then jointly optimized the RIS's

Table 1 Power minimization or EE maximization in RIS-assisted wireless networks

References	System setup	Objective	Design variables	Decoupling
[15]	MISO downlink	Min.transmit power	Transmit and passive beamforming	AO
[5]	MISO downlink-single carrier	Max. energy efficiency	Transmit and passive beamforming, On-off status of each RIS	AO
[16]	MISO downlink	Min.transmit power	Transmit beamforming, discrete phase control	AO
[17]	RIS-aided MISO downlink system	EE maximization	Active and passive beamforming	AO
[4]	MISO downlink-single carrier	Max. energy efficiency	Transmit and passive beamforming,	AO

passive beamforming and the BS's power distribution using the AO technique to increase the achievable rate. The authors in [14] integrate RIS into an orthogonal frequency division multiple access (OFDMA)-based multi-user (MU) downlink system. Joint optimization of the RIS's passive beamforming and OFDMA resource block (RB), as well as power allocations are leveraged to maximize the minimum user rate.

The goal of [15] is to minimize the AP's transmit power while taking into account the individual users' signal-to-interference-plus-noise ratio (SINR) restrictions by jointly optimizing the BS transmit beamforming and RIS's passive beamforming. The authors in [5] have used distributed RIS-enabled network to manage the RIS states. They investigate how to maximize EE by dynamically managing each RIS's on/off status and improving the reflection coefficients matrix of the RISs using two iterative techniques. In contrast, the paper proposed in [16] addresses the problem of minimizing transmit power in an RIS-aided wireless network with discrete phase shifts. The authors propose an AO technique as a suboptimal and low-complexity solution. Simulation results are provided to evaluate the performance compared to benchmark schemes. The authors in [17] present an optimization technique to maximize the EE of a RIS-aided system by jointly optimizing the BS's active beamforming and the RIS's passive beamforming. The proposed algorithm is shown to be effective through numerical results. The authors in [4] examined the maximization of EE in RIS-aided MISO systems. They tackled the problem by employing the gradient descent approach (GA). In each iteration of GA, they utilized a second-order approximation of the problem, assuming the convexity of the approximation. However, it is important to note that this assumption is not universally valid, as the objective function may not exhibit a shape resembling a second-order function. Therefore, to ensure that the optimization algorithm progresses in a decreasing manner, two line search strategies with the Wolfe condition and the trust region (TR) were employed in this paper. These strategies provide a guarantee of a monotonic decrease in the objective function values. Therefore, compared to the previously mentioned works, this paper addresses the limitations of existing optimization techniques when solving the EE problem in RIS-assisted communication networks. In this paper, we revisit the EE resource allocation problem in a RIS-assisted MISO communication system, focusing on overcoming the aforementioned limitations. As a result, the contributions of this paper can be summarized as follows:

- Due to concave nature of the problem at hand, the GA's success is not guaranteed. We, therefore, propose a Wolfe based gradient-descent algorithm (GAW) to solve the EE maximization problem with respect to RIS passive beamforming in the AO framework. The simulation results show that GAW improves the system's EE since using Wolf conditions in GAW guarantees a sufficient decrease in the objective function by producing an acceptable step size.
- We propose another novel approach using TR method for solving the EE problem with respect to RIS phase shifts design. By searching within a trust region, TR improves the search space of the problem compared to line search methods, which only search in a given direction. The improved search space helps TR to escape from saddle points [22, 23], resulting in better performance compared to GAW and other existing methods. Simulation results demonstrate the efficiency of the TR method.

Notation: The symbols $\boldsymbol{A}^T$, $\boldsymbol{A}^H$, $\boldsymbol{A}^{-1}$, $\boldsymbol{A}^+$, and $\|\boldsymbol{A}\|_F$ stand for the transpose, hermitian (conjugate transpose), inverse, pseudo-inverse, and Frobenius norm of a matrix $\boldsymbol{A}$, respectively. Besides, the functions $\mathcal{R}(\cdot)$, $\mathcal{I}(\cdot)$, $|\cdot|$, $(\cdot)^*$ and $\arg(\cdot)$ indicate distinct properties of a complex number, namely its real part, imaginary part, modulus, complex conjugate, and angle, in that order. The notation $\mathrm{tr}(\cdot)$ indicates the matrix trace, and $\boldsymbol{I}_n$(with $n \geq 2$) refers to the $n \times n$ identity matrix. To represent the Hadamard and Kronecker products of matrices $\boldsymbol{A}$ and $\boldsymbol{B}$, we use the symbols $\boldsymbol{A} \circ \boldsymbol{B}$ and $\boldsymbol{A} \otimes \boldsymbol{B}$, respectively. We use $vec(\boldsymbol{A})$ to denote a vector obtained by stacking all the columns of $\boldsymbol{A}$, and $\mathrm{diag}(a)$ represents a diagonal matrix with entries from vector a.

$\mathbb{R}$ and $\mathbb{C}$ stand for the sets of real and complex numbers, respectively, and the notation $x \sim \mathcal{CN}(0, \sigma^2)$ indicates that the random variable x follows a complex circularly symmetric Gaussian distribution with zero mean and variance σ^2.

2 Methods

2.1 System description and problem formulation

In this section, we provide an overview of the system model used in the RIS-assisted downlink multi-user MISO system. We also describe the formulation of the EE problem, which involves jointly optimizing the transmit powers and the phase shifts of the RIS.

2.1.1 System description

The system model, depicted in Fig. 1, consists of an M-antenna base station communicating with K single-antenna users via an RIS comprising N elements [4]. The RIS is installed on the exterior surface of a building that is located near both communication endpoints. Owing to adverse propagation conditions, the direct path between BS

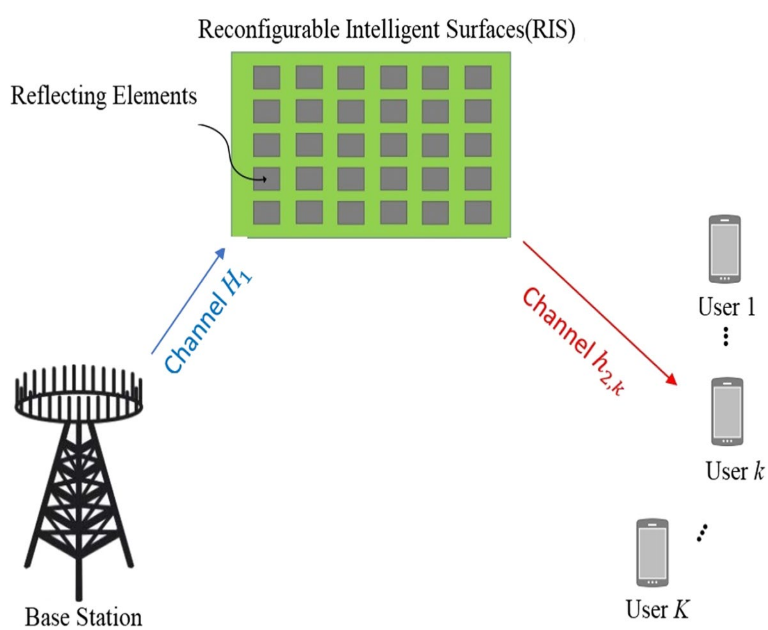

Fig. 1 The considered RIS-based multi-user MISO system

and mobile users is blocked. This RIS-assisted MISO communication model is widely described in [4, 11, 14].

The channel vector between the RIS and user k, the channel matrix between the BS and the RIS, and the diagonal matrix of RIS phase shifts, are denoted by $\boldsymbol{h}_{2,k} \in \mathbb{C}^{1\times N}$, $\boldsymbol{H}_1 \in \mathbb{C}^{N\times M}$, and $\boldsymbol{\Phi} = \text{diag}[\phi_1, \phi_2, \ldots, \phi_N]$, respectively, where $\phi_n = e^{j\theta_n}$ for all $n = 1, 2, \ldots, N$.

The transmitted signal is denoted by $\boldsymbol{x} = \sum_{k=1}^{K} \sqrt{p_k}\boldsymbol{g}_k s_k$, with p_k, s_k, and $\boldsymbol{g}_k \in \mathbb{C}^{M\times 1}$ representing, respectively, the transmit power, unit-power complex valued information symbol chosen from a discrete constellation set, and precoding vector of user k. The transmitted signal's power is also identified by $E[|\boldsymbol{x}|^2] = \text{tr}(\boldsymbol{P}\boldsymbol{G}^H\boldsymbol{G}) \le P_{\max}$, where $\boldsymbol{G} = [\boldsymbol{g}_1, \boldsymbol{g}_2, \ldots, \boldsymbol{g}_K] \in \mathbb{C}^{M\times K}$ and $\boldsymbol{P} = \text{diag}[p_1, \ldots, p_K] \in \mathbb{R}^{K\times K}$.

Subsequently, $y_k = \boldsymbol{h}_{2,k}\boldsymbol{\Phi}\boldsymbol{H}_1\boldsymbol{x} + w_k$ denotes the discrete-time signal received by mobile user k, where $k = 1, 2, \ldots, K$. The thermal noise power at receiver k is represented by $w_k \sim \mathcal{CN}(0, \sigma^2)$.

Next, the formula for the experienced SINR for k-th mobile user and the associated SE in bps/Hz is as follows:

$$\gamma_k = \frac{p_k \left|\boldsymbol{h}_{2,k}\boldsymbol{\Phi}\boldsymbol{H}_1\boldsymbol{g}_k\right|^2}{\sum_{i=1, i\neq k}^{K} p_i \left|\boldsymbol{h}_{2,k}\boldsymbol{\Phi}\boldsymbol{H}_1\boldsymbol{g}_i\right|^2 + \sigma^2}. \tag{1}$$

$$\text{SE} = \frac{\sum_{k=1}^{K} \log_2(1+\gamma_k)}{\text{B}}. \tag{2}$$

Consider the total power dissipation at an intelligent surface with N reflecting elements, denoted as P_{RIS}. It is given by the product of N and $P_n(b)$, where $P_n(b)$ represents the power consumption of a single phase shifter with b-bit resolution [4]. Therefore, the total power consumption of the system is represented as:

$$\mathcal{P}_{total} = \sum_{k=1}^{K} (\zeta p_k + P_{UE,k}) + P_{BS} + P_{\text{RIS}}, \tag{3}$$

where $\zeta = \nu^{-1}$ and ν represents the power amplifier's efficiency. Besides, $P_{UE,k}$, P_{BS}, P_{RIS} identifies the static power consumption of k-th user, BS, and RIS respectively.

2.1.2 Problem formulation

Consider $\boldsymbol{H}_2 = [\boldsymbol{h}_{2,1}^T, \boldsymbol{h}_{2,2}^T, \cdots, \boldsymbol{h}_{2,K}^T]^T \in \mathbb{C}^{K\times N}$. Then, assuming $M \ge K = N$, there exists a right inverse for $\boldsymbol{H}_2\boldsymbol{\Phi}\boldsymbol{H}_1$, which enables perfect interference suppression using the zero-forcing (ZF) beamforming scheme. The ZF precoding matrix $\boldsymbol{G} = (\boldsymbol{H}_2\boldsymbol{\Phi}\boldsymbol{H}_1)^+$ can then be used for this purpose. Substituting $\boldsymbol{G}$ in SINR formula (1, 2), the EE problem with respect to $\boldsymbol{P} = \text{diag}[p_1, p_2, \ldots, p_k]$ and $\boldsymbol{\Phi} = \text{diag}[\phi_1, \phi_2, \ldots, \phi_N]$ is formulated as follows:

$$\max_{\boldsymbol{\Phi}, \boldsymbol{P}} \quad \frac{\sum_{k=1}^{K} \log_2(1 + p_k\sigma^{-2})}{\xi \sum_{k=1}^{K} p_k + P_{BS} + KP_{UE} + P_{\text{RIS}}} \tag{4}$$

$$\text{subject to} \log_2\left(1+p_k\sigma^{-2}\right) \geq R_{min,k}, \forall k=1,2,\ldots,K, \tag{4a}$$

$$\mathrm{tr}((\mathbf{H}_2\Phi\mathbf{H}_1)^{+}\mathbf{P}(\mathbf{H}_2\Phi\mathbf{H}_1)^{+H}) \leq P_{max}, \tag{4b}$$

$$|\phi_n| = 1, \forall n=1,2,\ldots,N, \tag{4c}$$

where the interference is thought to be completely suppressed by the ZF precoding matrix. The EE problem in Eq. (4) is not easy to solve due to the coupling of $\boldsymbol{P}$ and $\boldsymbol{\Phi}$ in the second constraint and unit modulus constraint on $\boldsymbol{\Phi}$. In order to obtain a sub-optimal solution, alternating optimization is applied by splitting the problem (4) to two sub-problems with respect to $\boldsymbol{P}$ and $\boldsymbol{\Phi}$. As depicted in Table 1, many works have relied on AO to solve the EE optimization problem. However, the novelty of this paper relies in investigating the limitation of such a scheme that mainly relies on GA with non-guaranteed convergence.

2.2 Problem solution

The alternating optimization algorithm is employed to solve the problem according to the following steps:

- Optimization with respect to the RIS elements values $\boldsymbol{\Phi}$
- Optimization with respect to transmitted power $\boldsymbol{P}$.

2.2.1 Optimization with respect to the RIS element values $\boldsymbol{\Phi}$

For the fixed values of $\boldsymbol{P}$, the problem (4) is converted to the following problem:

$$\max_{\boldsymbol{\Phi}} \quad C_o \tag{5}$$

$$\text{subject to} \quad \mathrm{tr}((\mathbf{H}_2\Phi\mathbf{H}_1)^{+}\mathbf{P}(\mathbf{H}_2\Phi\mathbf{H}_1)^{+H}) \leq P_{max}, \tag{5a}$$

$$|\phi_n| = 1, \forall n=1,2,\ldots,N, \tag{5b}$$

within this context, C_o represents an arbitrary constant value. Then, Eq. (5) reformulated as an unconstrained problem as follows:

$$\begin{aligned}\min_{\boldsymbol{\Theta}} \mathcal{F}(\boldsymbol{\Phi}(\boldsymbol{\Theta})) &= \mathrm{tr}((\boldsymbol{H}_2\boldsymbol{\Phi}(\boldsymbol{\Theta})\boldsymbol{H}_1)^{+}\boldsymbol{P}(\boldsymbol{H}_2\boldsymbol{\Phi}(\boldsymbol{\Theta})\boldsymbol{H}_1)^{+\mathrm{H}}) \\ &= \mathrm{vec}(\boldsymbol{\Phi}^{-1}(\boldsymbol{\Theta}))^{\mathrm{H}}(\overline{\boldsymbol{H}}_2^{+\mathrm{H}} \otimes \boldsymbol{H}_1^{+})^{\mathrm{H}}(\overline{\boldsymbol{H}}_2^{+\mathrm{H}} \otimes \boldsymbol{H}_1^{+})\mathrm{vec}(\boldsymbol{\Phi}^{-1}(\boldsymbol{\Theta})),\end{aligned} \tag{6}$$

where $\boldsymbol{\Theta} = \mathrm{diag}[\theta_1, \theta_2, ..., \theta_N]$, $\boldsymbol{\Phi} = \mathrm{diag}[e^{j\theta_1}, e^{j\theta_2}, ..., e^{j\theta_N}]$, $\boldsymbol{P} = \boldsymbol{Q}\boldsymbol{Q}^T$ and $\overline{\boldsymbol{H}}_2 = \boldsymbol{Q}^{-1}\boldsymbol{H}_2$. We proposed two efficient approach to solve the problem in Eq. (6) that will be described in the next subsections.

Gradient Descent Approach

The gradient descent method can be applied for solving the problem in Eq. (6) .

GA as a line search algorithm minimizes the linear approximation of $f(x)$ by first calculating a search direction, $s^{(t)}$, and then deciding how far to move in that direction. The GA iterates as follows:

$$x^{(t+1)} = x^{(t)} + \alpha^{(t)} s^{(t)}, \tag{7}$$

where $\alpha^{(t)}$ is step size. For the line search method to be effective, the direction $s^{(t)}$ and step length $\alpha^{(t)}$ must be carefully selected [22].

So, considering the problem in Eq. (6), the following matrices are defined:

$$\boldsymbol{A} = (\overline{\boldsymbol{H}}_2^{+H} \otimes \boldsymbol{H}_1^{+})^H (\overline{\boldsymbol{H}}_2^{+H} \otimes \boldsymbol{H}_1^{+}) \in \mathbb{C}^{N^2 \times N^2}, \tag{8}$$

$$\boldsymbol{y} = vec(\boldsymbol{\Phi}^{-1}(\boldsymbol{\Theta})) \in \mathbb{C}^{N^2 \times 1}, \tag{9}$$

so that,

$$\mathcal{F}(\boldsymbol{\Phi}(\boldsymbol{\Theta})) = \boldsymbol{y}^H \boldsymbol{A} \boldsymbol{y}, \tag{10}$$

in which

$$\boldsymbol{y}^H \boldsymbol{A} \boldsymbol{y} = \sum_{n=1}^{N} a_{l(n),l(n)} + 2\mathcal{R}\left\{ \sum_{n=1}^{N} \sum_{m \geq n}^{N} a_{l(n),l(m)} e^{j(\theta_n - \theta_m)} \right\}, \tag{11}$$

where $l(n)$ is the index map $l(n) = (n-1)N + n$, for all $n = 1, \ldots, N$, and $a_{l(n),l(m)}$ denotes the $l(n)$, $l(m)$-th element of $\boldsymbol{A}$. By substituting $\alpha^{(t)}$ and $s^{(t)}$ in Eq. (7) with μ and $\boldsymbol{d}^{(t)}$ respectively, the iteration of the gradient descent approach for the problem in Eq. (6) can be expressed as:

$$vec(\boldsymbol{\Theta})^{(t+1)} = vec(\boldsymbol{\Theta})^{(t)} + \mu \boldsymbol{d}^{(t)}, \tag{12}$$

and

$$\boldsymbol{y}^{(t+1)} = \exp(j \cdot \mathrm{vec}(\boldsymbol{\Theta})^{(\mathrm{t+1})}) \circ \mathrm{vec}(\boldsymbol{I}_{\mathrm{N}}) = \boldsymbol{y}^{(\mathrm{t})} \circ \exp(\mathrm{j}\mu \boldsymbol{d}^{(\mathrm{t})}), \tag{13}$$

where $vec(\boldsymbol{\Theta})^{(t)}$ is the phase of $\boldsymbol{y}$ at iteration t [4].

The descent direction is updated using the Polak-Ribiere-Polyak conjugate gradient algorithm according to the following formula:

$$\boldsymbol{d}^{(t+1)} = -\boldsymbol{q}^{(t+1)} + \frac{(\boldsymbol{q}^{(t+1)} - \boldsymbol{q}^{(t)})^T \boldsymbol{q}^{(t+1)}}{\|\boldsymbol{q}^{(t)}\|^2} \boldsymbol{d}^{(t)}, \tag{14}$$

where $\boldsymbol{q}^{(t+1)}$ for the first iteration of the algorithm is obtained as follows:

$$\begin{aligned} -\nabla_{\boldsymbol{\Theta}}(\boldsymbol{y}^H \boldsymbol{A} \boldsymbol{y}) = 2\mathcal{R}\Big\{ & j e^{j\theta_i} \sum_{m>i}^{N} a_{l(i),l(m)} e^{-j\theta_m} \\ & - j e^{-j\theta_i} \sum_{n<i}^{N} a_{l(n),l(i)} e^{j\theta_n} \Big\}. \end{aligned} \tag{15}$$

Next, to ensure that it is a descent direction, the following formula should be checked:

$$\boldsymbol{d}^{(t+1)} = \begin{cases} \boldsymbol{d}^{(t+1)} & : \ (\boldsymbol{q}^{(t+1)})^T \boldsymbol{d}^{(t+1)} < 0 \\ -\boldsymbol{q}^{(t+1)} & : \ (\boldsymbol{q}^{(t+1)})^T \boldsymbol{d}^{(t+1)} \geq 0. \end{cases} \tag{16}$$

In the subsequent subsections, two approaches based on Wolfe condition and trust region are proposed. The limitations of the GA is addressed in details in section IV.

Wolfe Condition Based GA

A common inexact line search condition mandates that $\alpha^{(t)}$ in Eq. (7) must first sufficiently reduce the objective function *f*. Wolfe conditions, including the Armijo condition and the curvature condition (CC), can be used to achieve this adequate reduction where their formulation is as follows [22]:

- Armijo Condition

$$\begin{aligned} \mathcal{F}(\boldsymbol{\Phi}(\boldsymbol{\Theta}^{(t+1)})) \leq & \ \mathcal{F}(\boldsymbol{\Phi}(\boldsymbol{\Theta}^{(t)})) \\ & + c_1 \mu (\boldsymbol{d}^{(t)})^T \nabla_{\boldsymbol{\Theta}} \mathcal{F}(\boldsymbol{\Phi}(\boldsymbol{\Theta}))|_{\boldsymbol{\Theta}=\boldsymbol{\Theta}^{(t)}}. \end{aligned} \tag{17}$$

- Curvature Condition

$$(\boldsymbol{d}^{(t)})^T \nabla_{\boldsymbol{\Theta}} \mathcal{F}(\boldsymbol{\Phi}(\boldsymbol{\Theta}))|_{\boldsymbol{\Theta}=\boldsymbol{\Theta}^{(t+1)}} \geq c_2 (\boldsymbol{d}^{(t)})^T \nabla_{\boldsymbol{\Theta}} \mathcal{F}(\boldsymbol{\Phi}(\boldsymbol{\Theta}))|_{\boldsymbol{\Theta}=\boldsymbol{\Theta}^{(t)}}. \tag{18}$$

Armijo condition ensures that the algorithm is making sufficient progress in each iteration towards the optimal solution. By requiring a minimum decrease in the objective function value, the algorithm avoids taking overly conservative steps that may converge slowly. The curvature condition ensures that the search direction points towards the optimal solution, rather than away from it. By requiring that the search direction is a descent direction, the algorithm ensures that it is moving towards the optimal solution in each iteration.

Trust-Region Method Trust-region methods use a quadratic model of the objective function to generate steps. These methods define a region around the current solution and trust that the model is a good representation of the objective function within this region. The method then simultaneously selects the direction and length of the step by approximating the minimizer of the model in this region. If the step is not acceptable, the trust region size is reduced and a new minimizer is found. The direction of the step changes whenever the size of the trust region is changed. The size of the trust region is critical to the effectiveness of the method because if it is too small, a significant step opportunity can be missed, and if it is too large, the model minimizer may be far from the objective function minimizer in the region, necessitating the reduction of the trust region size and go over another attempt. This method utilizes Algorithm 5 and applies it to the merit function:

$$F(\boldsymbol{\Phi}(\boldsymbol{\Theta})) = \frac{1}{2} \left\| (\overline{\boldsymbol{H}}_2^{+H} \otimes \boldsymbol{H}_1^{+}) vec(\boldsymbol{\Phi}^{-1}(\boldsymbol{\Theta})) \right\|_2^2 = \frac{1}{2} \left\| \boldsymbol{B}\boldsymbol{y} \right\|_2^2 = \frac{1}{2} \| \boldsymbol{r}(\boldsymbol{\Theta}) \|_2^2, \tag{19}$$

where $\boldsymbol{B} = (\overline{\boldsymbol{H}}_2^{+H} \otimes \boldsymbol{H}_1^{+}) \in \mathbb{C}^{N^2 \times N}$ and $\boldsymbol{y} = vec(\boldsymbol{\Phi}^{-1}(\boldsymbol{\Theta})) \in \mathbb{C}^{N^2 \times 1}$. The model function $m^{(t)}(\boldsymbol{s})$ is usually defined as follows:

$$m^{(t)}(\boldsymbol{s}) = \frac{1}{2}\left\|\boldsymbol{r}^{(t)} + \boldsymbol{J}^{(t)}\boldsymbol{s}\right\|_2^2 = f^{(t)} + \boldsymbol{s}^T(\boldsymbol{J}^{(t)})^T\boldsymbol{r}^{(t)} + \frac{1}{2}\boldsymbol{s}^T(\boldsymbol{J}^{(t)})^T\boldsymbol{J}^{(t)}\boldsymbol{s}^{(t)}, \tag{20}$$

Where $\boldsymbol{r}^{(t)} = r(\boldsymbol{\Phi}(\boldsymbol{\Theta}))|_{\boldsymbol{\Theta}=\boldsymbol{\Theta}^{(t)}}$, $\boldsymbol{J}^{(t)} = \nabla^T \boldsymbol{r}^{(t)}(\boldsymbol{\Phi}(\boldsymbol{\Theta}))$ and $\boldsymbol{B}^{(t)} = (\boldsymbol{J}^{(t)})^T\boldsymbol{J}^{(t)}$ is an approximation of the Hessian matrix. Considering $\boldsymbol{B} = \left[b_{ij}\right] \in \mathbb{C}^{N^2 \times N}$, the Jacobian of the $r(\boldsymbol{\Theta})$ is formulated as follows:

$$\boldsymbol{J}(\boldsymbol{\Phi}(\boldsymbol{\Theta})) = \left[-jb_{n,L(m)} \exp(-j\theta_m)\right], \tag{21}$$

where $L(m) = (m-1)N + m$.

Then, the step $\boldsymbol{s}^{(t)}$ is obtained by solving the following sub-problem:

$$\min_{s} \quad m^{(t)}(\boldsymbol{s}) \tag{22}$$

$$\text{subject to} \quad \|\boldsymbol{s}\| \leq \overset{(t)}{\triangle}, \tag{22a}$$

where the scalar $\triangle > 0$ is called the trust-region radius. A crucial aspect in several trust-region algorithms is the ratio $\rho^{(t)}$, which represents the actual reduction to predicted reduction. Its value is determined as follows:

$$\rho_t = \frac{F(\boldsymbol{\Phi}(\boldsymbol{\Theta}^{(t)})) - F(\boldsymbol{\Phi}(\boldsymbol{\Theta}^{(t)} + s^{(t)}))}{m^{(t)}(0) - m^{(t)}(s^{(t)})}. \tag{23}$$

If the obtained $\boldsymbol{s}^{(t)}$ does not result in a significant reduction in $F(\boldsymbol{\Phi}(\boldsymbol{\Theta}))$, it will result in a trust region being too large and shrink it before solving the problem in Eq. (22) again.

2.2.2 Optimization with respect to the transmitted power P

Solving the EE problem, with respect to the transmit power $\boldsymbol{P}$ for a fixed RIS phase shift matrix, rely on the Dinkelbach algorithm [4]. The Dinkelbach algorithm, known as a powerful fractional programming tool, is widely employed for optimizing wireless networks, as evidenced by its application in various studies [23–26].

The Backtracking line search algorithm, the trust region method, the GAW-based EE maximization algorithm, and the TR-based EE maximization algorithm are outlined in Tables 2, 3, 4, and 5, respectively.

Table 2 Backtracking line search

Algorithm 1. Backtracking Line Search
1. **Input**: $\overline{\mu} > 0, \rho \in (0,1), c_1 \in (0,1), c_2 \in (0,1)$.
2. Set $\mu_t = \overline{\mu}$,
3. If (17) and (18) are satisfied, stop and $\mu_t = \mu$.
4. Otherwise $\mu_t = \rho\mu$ and go to step 3.

Table 3 Trust region method

Algorithm 2. Trust Region Method

1. **Input**: $\overline{\triangle} > 0, \triangle^0 \in (0, \overline{\triangle})$, and $\eta \in [0, \frac{1}{4})$:
2. **For** $t = 0, 1, 2, \ldots$
3. Calculate $s^{(t)}$ as an (approximate) solution of (22).
4. Evaluate $\rho^{(t)}$.
5. **if** $\rho^{(t)} < \frac{1}{4}$
6. $\triangle^{(t+1)} = \frac{1}{4}\|s^{(t)}\|$.
7. **else**
8. **if** $\rho^{(t)} > \frac{3}{4}$ and $\|s^{(t)}\| = \triangle^{(t)}$
9. $\triangle^{(t+1)} = \min(2\triangle^{(t)}, \overline{\triangle})$.
10. **else**
11. $\triangle^{(t+1)} = \triangle^{(t)}$;
12. **end (if)**
13. **end (if)**
14. **if** $\rho^{(t)} > \eta$
15. $x^{(t+1)} = x^{(t)} + s^{(t)}$.
16. **else**
17. $x^{(t+1)} = x^{(t)}$.
18. **end (if)**
19. **end (for)**.

Table 4 GAW-based EE maximization algorithm

Algorithm 3. GAW-based EE Maximization Algorithm

1. **Input**: $K, n, \eta, P_{\mathsf{Bs}}, P_{\mathsf{UE}}, P_n(b), P_{\mathsf{max}}$, σ^2, $\{R_{\mathsf{min},k}\}_{k=1}^{K}$, $\mathbf{H}_2$, $\mathbf{H}_1$, $\epsilon > 0$,
2. **Initialization**: $p^0 = \frac{P_{\mathsf{max}}}{K} \cdot I_K$, $\mathbf{\Phi}_0 = \frac{\pi}{2} \cdot I_N$, $q_0 = \nabla_{\boldsymbol{\theta}}((\mathbf{y}^0)^H \mathbf{A}\mathbf{y}^0)$, and $\mathbf{d}^0 = -\mathbf{q}^0$,
3. **While** $\left|EE^{(l+1)} - EE^{(l)}\right|^2 > \epsilon$, **do**
4. Given $\mathbf{P}$, update $\mathbf{\Phi}$,
5. **For** $t = 0, 1, 2, \cdots$ **do**,
6. Obtain step size μ_t using Algorithm 1,
7. $\mathbf{y}^{t+1} = \mathbf{y}^t \circ \exp^{j\mu \mathbf{d}^t} \circ \mathrm{vec}(\mathbf{I}_N)$,
8. $\mathbf{q}^{t+1} = 2\mathrm{Real}(-j(\mathbf{y}^*)^{t+1} \circ (\mathbf{A}\mathbf{y}^{t+1}))$,
9. $\mathbf{d}^{t+1} = -\mathbf{q}^{t+1} + \frac{(\mathbf{q}^{t+1} - \mathbf{q}^t)^T \mathbf{q}^{t+1}}{\|\mathbf{q}^t\|} \mathbf{d}^t$.
10. $\mathbf{d}^{t+1} = \begin{cases} \mathbf{d}^{t+1} & : \ (\mathbf{q}^{t+1})^T \mathbf{d}^{t+1} < 0 \\ -\mathbf{q}^{t+1} & : \ (\mathbf{q}^{t+1})^T \mathbf{d}^{t+1} \geq 0 \end{cases}$,
11. **Until** $\left\|\mathbf{\Phi}^{(t+1)} - \mathbf{\Phi}^t\right\|^2 < \epsilon$, Obtain $\mathbf{\Phi}^{(l+1)} = \mathbf{\Phi}^{(t+1)}$.
12. **end For**
13. Given $\mathbf{\Phi}$ update $\boldsymbol{P}$:
14. **if** $\mathrm{tr}((\boldsymbol{H}_2\mathbf{\Phi}\boldsymbol{H}_1)^+ \boldsymbol{P} (\boldsymbol{H}_2\mathbf{\Phi}\boldsymbol{H}_1)^{+H})$ evaluated at $\mathbf{\Phi}^{(l+1)}$ is lower than P_{max} **then**:
15: Update P by solving the following problem using Dinkelbach's Method:

$$\boldsymbol{P}^{l+1} = \arg max_{\boldsymbol{P} \in \mathcal{B}} \frac{\sum_{k=1}^{K} \log_2(1 + p_k \sigma^{-2})}{\xi \sum_{k=1}^{K} p_k + P_{BS} + K P_{UE} + N P_n(b)}$$

16: **else** Break and declare infeasibility.
17: **end if**
18: **end while**
19: **Output**: $\mathbf{\Phi}$ and $\boldsymbol{P}$

Table 5 TR-based EE maximization algorithm

Algorithm 4. TR-based EE Maximization Algorithm

1. **Input**: $K, n, \eta, P_{Bs}, P_{UE}, P_n(b), P_{max}, \sigma^2, \{R_{min,k}\}_{k=1}^{K}$, $\boldsymbol{H_2}, \boldsymbol{H_1}$, $\epsilon > 0$.
2. **Initialization**: $p^0 = \frac{P_{max}}{K} * I_K, \boldsymbol{\Phi}_0 = \frac{\pi}{2} * I_N, q_0 = \nabla_{\boldsymbol{\theta}} = ((\boldsymbol{y}^0)^H \boldsymbol{A}\boldsymbol{y}^0)$, and $\boldsymbol{d}^0 = -\boldsymbol{q}^0$.
3. **While** $\left|EE^{(l+1)} - EE^{(l)}\right|^2 > \epsilon$, **do**
4. Given $\mathbf{P}$, update $\boldsymbol{\Phi}$ using Algorithm 5.
5. **Until** $\left\|\boldsymbol{\Phi}^{(t+1)} - \boldsymbol{\Phi}^t\right\|^2 < \epsilon$, Obtain $\boldsymbol{\Phi}^{(l+1)} = \boldsymbol{\Phi}^{(t+1)}$.
6. Given $\boldsymbol{\Phi}$ update $\boldsymbol{P}$:
7. **if** $\operatorname{tr}((\boldsymbol{H}_2\boldsymbol{\Phi}\boldsymbol{H}_1)^+ \boldsymbol{P}(\boldsymbol{H}_2\boldsymbol{\Phi}\boldsymbol{H}_1)^{+H})$ evaluated at $\boldsymbol{\Phi}^{(l+1)}$ is lower than P_{max} then:
8: Update P by solving the following problem using Dinkelbach's Method: $\boldsymbol{P}^{(l+1)} = \arg max_{\boldsymbol{P}\in\mathcal{B}} \frac{\sum_{k=1}^{K} \log_2(1+p_k\sigma^{-2})}{\xi \sum_{k=1}^{K} p_k + P_{BS} + KP_{UE} + NP_n(b)}$
9. **else** Break and declare infeasibility.
10. **end if**
11. **end while**
12. **Output**: $\boldsymbol{\Phi}$ and $\boldsymbol{P}$

3 Results and discussion

In this section, we present the results of our study and provide a comprehensive discussion of the findings.

3.1 Discussion: Investigating the limitation of the GA and the convergence rate

In the following subsection, we analyze the drawbacks of the GA and conduct a comprehensive assessment of its convergence rate, shedding light on its effectiveness in solving the optimization problem.

3.1.1 Investigating the limitation of the GA

The gradient descent approach solves the following minimization problem to obtain the step length.

$$\min_{\mu>0} h(\mu) = (\boldsymbol{y}^{(t+1)})^H \boldsymbol{A}\boldsymbol{y}^{(t+1)}, \tag{24}$$

where

$$h(\mu) = \sum_{n=1}^{N} a_{l(n),l(n)} + 2\mathcal{R}\{\sum_{n=1}^{N}\sum_{m>n}^{N} a_{l(n),l(m)} e^{j(\theta_n^{(t)} - \theta_m^{(t)})} e^{j(d_m^{(t)} - d_n^{(t)})}\}. \tag{25}$$

In order to reduce the complexity, the authors in [4], consider a quadratic approximation of Eq. (25) by considering the second order Taylor expansion of the term $e^{j\mu(d_m^{(t)} - d_n^{(t)})}$ around $\mu = 0$, which yields the following approximation of $h(\mu)$:

$$\begin{aligned} \hat{h}(\mu) = \sum_{n=1}^{N} a_{l(n),l(n)} &+ 2\mathcal{R}\{\sum_{n=1}^{N}\sum_{m>n}^{N} a_{l(n),l(m)} e^{j(\theta_n^{(t)} - \theta_m^{(t)})} \\ &\times (1 + j\mu(d_m^{(t)} - d_n^{(t)}) + \frac{(J\mu(d_m^{(t)} - d_n^{(t)}))^2}{2})\}, \end{aligned} \tag{26}$$

Table 6 Limitations of GA in determining optimal step size

Monte Carlo #2, $N = 4$	Z_2	Monte Carlo, #2 $N = 20$	Z_2
AO #2	8.0169×10^{-6}	AO #2	0.0014
AO #2	5.1880×10^{-6}	AO #2	9.8480×10^{-4}
AO #2	2.7067×10^{-6}	AO #2	1.6767×10^{-4}
AO #3	8.1225×10^{-4}	AO #3	1.8284×10^{-6}
AO #3	4.1678×10^{-5}	AO #3	1.3191×10^{-6}

which can be expressed in a simple form as:

$$\hat{h}(\mu) = z_0 + z_1\mu - z_2\mu^2, \tag{27}$$

where the value of μ^* is given by $\mu^* = \frac{z_1}{(2z_2)}$. For μ^* to be a minimizer, the constraint $\mu > 0$ must be satisfied. This requires z_1 and z_2 to have the same sign. The relation between convexity of $\hat{h}(\mu)$ and the condition for μ^* to be a maximum or minimum is as follows:

$$\hat{h}''(\mu) = -2z_2 = \begin{cases} \hat{h}''(\mu) > 0 \text{ Minimizer,} \\ \hat{h}''(\mu) < 0 \text{ Maximizer,} \\ \hat{h}''(\mu) = 0 \text{ Indeterminate,} \end{cases} \tag{28}$$

where $\hat{h}''(\mu)$ is the second-order derivative of $\hat{h}(\mu)$. As a result, it is not appropriate to use the condition $\hat{h}''(\mu) < 0$ or $z_2 > 0$, as this may lead to incorrect results. Also, if $z_2 < 0$ but $z_1 > 0$, the resulting μ will be negative, even though a positive step size is acceptable.

While simulating the GA-based EE maximization algorithm, it was found that the case $z_2 > 0$ does occur, as shown in Table 6 for different number of RIS elements and AO iterations (Monte Carlo iterations). Moreover, the approximation of the exponential function with a second-order function may not be appropriate for obtaining the step size, as the values of the functions may be significantly different around $\mu = 0$.

3.1.2 Complexity and convergence rate

In this subsection, we discuss the comparsion of CPU time and convergence rate of the gradient descent, gradient descent with Wolfe condition, and trust region methods.

Gradient descent: Gradient descent is a widely used optimization algorithm that iteratively updates the solution by taking steps in the direction of the negative gradient of the objective function. The step size is usually determined by a fixed learning rate, which can be tuned for optimal performance. Gradient descent can be computationally efficient, but its convergence rate can be slow, especially for ill-conditioned or non-convex problems.

Gradient descent with Wolfe condition: Gradient descent with Wolfe condition is a variant of gradient descent that uses a line search to determine the step size at each iteration. The Wolfe condition ensures that the objective function decreases sufficiently at each iteration, which can improve the convergence rate compared to standard gradient descent. However, the line search can add additional computational overhead, which can make this method slower than standard gradient descent.

Trust region methods: Trust region methods are a family of optimization algorithms that aim to find the optimal solution within a trust region around the current point. At each iteration, a quadratic model of the objective function is constructed and solved within the trust region. This approach can lead to faster convergence and better accuracy than gradient descent or gradient descent with Wolfe condition, especially for highly non-convex or ill-conditioned problems. However, the trust region sub-problem can be computationally expensive to solve, which can make this method slower than standard gradient descent or gradient descent with Wolfe condition.

The convergence rate and complexity of gradient descent with the Wolfe condition, as well as trust region method, are examined in the following through the utilization of mathematical theorems.

Gradient Descent

- Complexity For the nonconvex optimization problem, it is known that the gradient method finds an ϵ-stationary point (i.e., the point satisfies $\|\nabla\mathcal{F}\| \leq \epsilon$) after at most $o(\epsilon^{-2})$ iterations. When applied to convex optimization, the gradient method [27] drove an interation complexity bound $o(\epsilon^{-1})$.
- Convergence rate

Consider the following assumption:

Assumption 1 (i) The level set $\mathcal{L} := \{\boldsymbol{\Theta} : \mathcal{F}(\boldsymbol{\Phi}(\boldsymbol{\Theta})) \leq \mathcal{F}(\boldsymbol{\Phi}(\boldsymbol{\Theta}^{(0)}))\}$ is bounded. (ii) In some neighborhood $\mathcal{N}$ of $\mathcal{L}$, the objective function F is continuously differentiable, and its gradient is Lipschitz continuous i.e. there exists a constant $L > 0$ such that

$$||\nabla\mathcal{F}(\boldsymbol{\phi}(\boldsymbol{\theta})) - \nabla\mathcal{F}(\boldsymbol{\phi}(\tilde{\boldsymbol{\theta}}))|| \leq L||\theta - \tilde{\theta})||. \tag{29}$$

Theorem 1 [28] *Suppose that Assumptions 1 hold. Consider the Polak-Ribiere method with a line search satisfying the Wolfe conditions* (17)-(18) *and the sufficient descent condition* $\left\langle \boldsymbol{d}^{(t)}, \boldsymbol{q}^{(t)} \right\rangle \leq \sigma \left\|\boldsymbol{q}^{(t)}\right\|^2$for some $\quad 0 < \sigma \leq 1$. *Then,*

$$\lim_{t\to\infty} \inf \mathcal{F}(\boldsymbol{\Phi}(\boldsymbol{\Theta}^{(t)}) = 0. \tag{30}$$

Regarding the rate of convergence of gradient descent with the Wolfe condition, many theories typically make the assumption that the line search is exact, meaning that:

$$\mu_k = \arg\min_{\mu}(\mathcal{F}(\boldsymbol{\Phi}(\boldsymbol{\Theta}^{(t+1)})), \tag{31}$$

where [29] shows that in fact:

$$\left\|\boldsymbol{\Theta}^{(t+n)} - \boldsymbol{\Theta}^*\right\| = O(\left\|\boldsymbol{\Theta}^{(t)} - \boldsymbol{\Theta}^*\right\|^2). \tag{32}$$

Trust region

- Complexity An early result of [30] shows that standard trust-region methods require $O(\epsilon_g^{-2})$ iterations to find an ϵ_g-stationary point; and given a (small) real positive tolerance ϵ_g, the algorithm terminate when it finds a point $\mathbf{\Theta}^{\epsilon}$ such that

$$\left\|\nabla\mathcal{F}(\mathbf{\Phi}(\mathbf{\Theta}^{\epsilon}))\right\| \leq \epsilon_g.$$

- Convergence rate The following theorem explains the global convergence of trust-region Newton methods.

Theorem 2 [22] *Let $\eta \in (0, \frac{1}{4})$ in step 1 of the algorithm presented in Table 3. Suppose that $||B^{(t)}|| \leq \beta$ for some constant β, that $\mathcal{F}$ is bounded below on the level set $S = \{\boldsymbol{\theta}|\mathcal{F}(\phi(\boldsymbol{\theta})) \leq \mathcal{F}(\phi(\boldsymbol{\theta}^{(\mathbf{0})}))\}$ and Lipschitz continuously differentiable in $S(R_0)$ for some $R_0 > 0$ (Eq. (34)), and that all approximate solutions $s^{(t)}$ of Eq. (20) satisfy the inequalities in Eq. (35) and $||s^{(t)}|| \leq \gamma\Delta^{(t)}$for some positive constants c and $\gamma \geq 1$. We then have*

$$\lim_{t\to\infty}\left(J^{(t)}\right)^T\gamma^{(t)} = 0. \tag{33}$$

$$S(R_0) = \{\boldsymbol{\theta}|\left\|\boldsymbol{\theta} - \bar{\boldsymbol{\theta}}\right\| < R_0 \quad \text{for some} \quad \bar{\boldsymbol{\theta}} \in S\}. \tag{34}$$

$$m^{(t)}(0) - m^{(t)}(s) \geq c\left\|(J^{(t)})^T\gamma^{(t)}\right\| \min\left(\Delta^{(t)}, \frac{\left\|(J^{(t)})^T\gamma^{(t)}\right\|}{\left\|B^{(t)}\right\|}\right). \tag{35}$$

The following theorem explains the local convergence of trust-region Newton methods.

Theorem 3 [[22]] *Let F be twice Lipschitz continuously differentiable in a neighborhood of a point $\boldsymbol{\theta}^*$ at which second-order sufficient conditions are satisfied. Suppose the sequence $\boldsymbol{\theta}^{(t)}$ converges to $\boldsymbol{\theta}^*$ and that for all t sufficiently large, the trust-region algorithm based on (22) chooses steps $s^{(t)}$ that satisfy Eq. (35) and are asymptotically similar to Newton steps $\mathbf{e}_k^N$ in (37) whenever $\left\|\mathbf{e}_k^N\right\| \leq \frac{1}{2}\Delta^{(t)}$, that is,*

$$\left\|s^{(t)} - \mathbf{e}_k^N\right\| = o\left(\left\|\mathbf{e}_k^N\right\|\right). \tag{36}$$

$$\mathbf{B}^{(t)}\mathbf{e}_k^N = -\left(\mathbf{J}^{(t)}\right)^T\boldsymbol{\gamma}^{(t)}. \tag{37}$$

Then the trust-region bound $\Delta^{(t)}$ becomes inactive for all t sufficiently large, and the sequence $\boldsymbol{\theta}^{(t)}$ converges superlinearly to $\boldsymbol{\theta}^*$.

3.2 Simulation results

In this sub-section, we investigate the performance of the RIS-assisted K-user MISO communication system. The channels are generated according to the 3GPP propagation environment described in [32]. An average of 10^3 independent realizations of the users' positions and channel realizations are used in the simulations. In addition, similar individual rate constraints for all K users are considered. $R_{\mathrm{min,k}} = R_{\mathrm{min}}$, for all k is considered where R_{min} is a fraction of the rate that each user would have in the genie case of mutually orthogonal channels and uniform power allocation. The genie rate is described as $R = \log_2(1 + \frac{P_{\max}}{K\sigma^2})$. Other simulation parameters are shown in

Table 7 Simulation parameters

Parameters	Values
Bandwidth of the BS B	180 KHz
Maximum transmit power of the AF relay P_R	20 dBm
Small scale fading model $\forall k, i$, and$j$	$[\mathbf{H}_{1_{i,j}}], [\mathbf{h}_{2_{k,i}}] \sim \mathcal{CN}(0, 1)$.
Large scale fading model at distance d	$\frac{10^{-3.53}}{d^{3.76}}$
Circut power of the Bs P_B	39 dBm
Circut disspitated power coefficients at the Bs/AF relay $\nu\, P_B$	1.2
Circut power of each user P_k	10 dBm
Circut power of each RIS element P_R	10 dBm
Circut power of each AF relay transmit-receive antenna element P_A	10 dBm

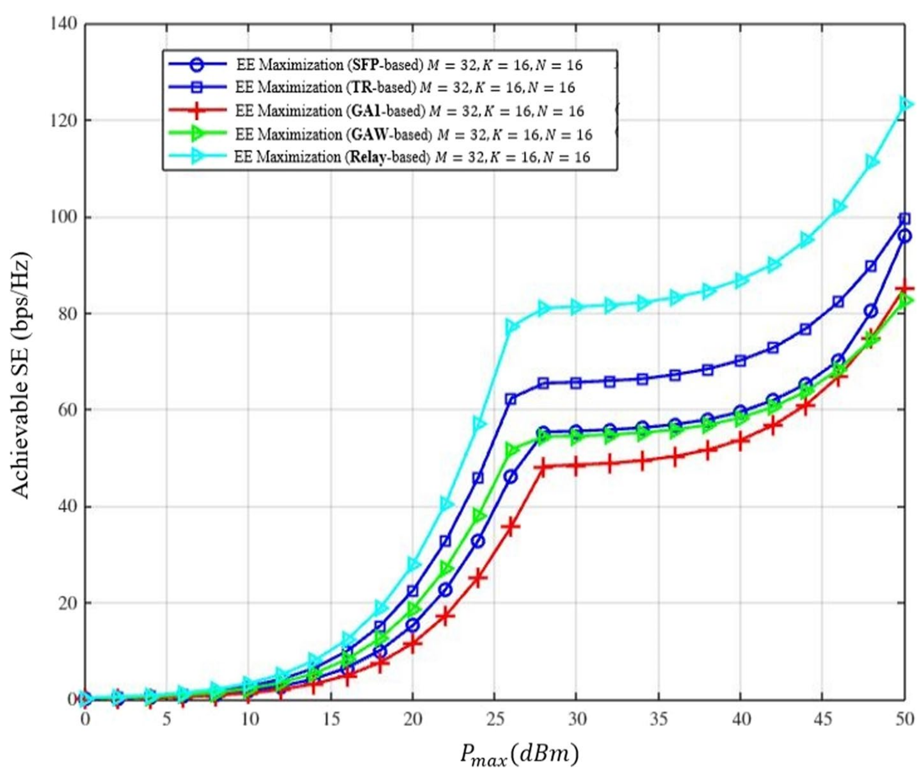

Fig. 2 Average SE using either RIS or AF relay versus $P_{\max}$ for $R_{\min} = 0.2$ bps/Hz and $M = 32, K = 16, N = 16$

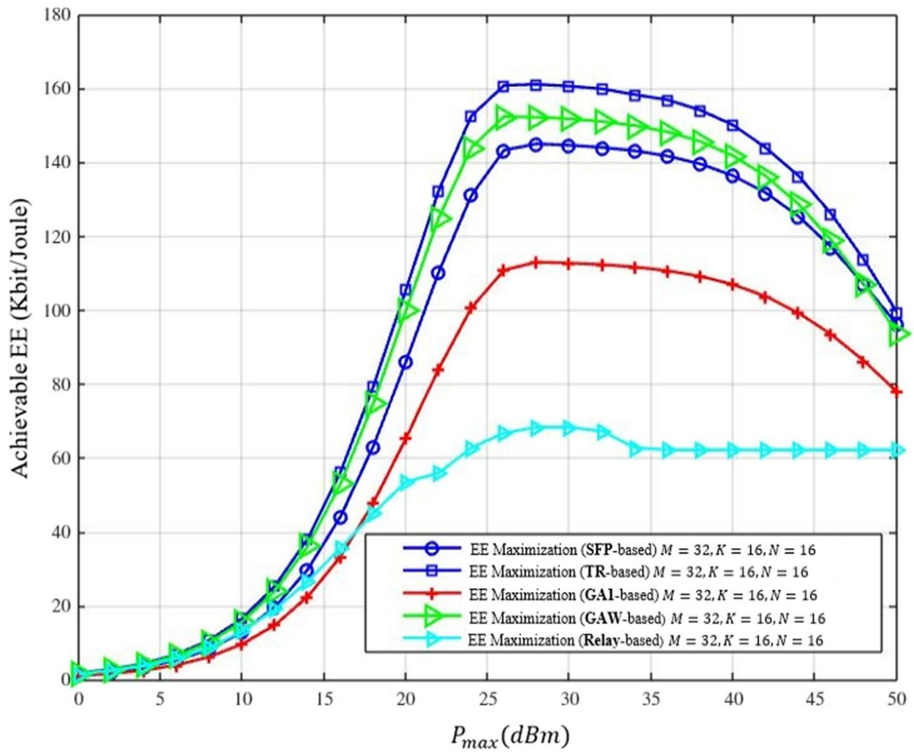

Fig. 3 Average EE using either RIS or AF relay versus $P_{\max}$ for $R_{\min} = 0.2$ bps/Hz and $M = 32, K = 16, N = 16$

Table 7. The achievable SE and EE performances as functions of $P_{\max}$ in dBm are illustrated in Figs. 2 and 3, respectively. We evaluated the proposed GAW- and TR-based approaches for EE maximization. Additionally, we considered the frequently referenced model-based benchmark approaches, such as the GA-based, SFP-based, and amplify-and-forward (AF) relay-based method [4] . In both figures, we have set the minimum QoS constraint as $R_{\min} = 0.2$ bps/Hz for all K users, and considered the setting $M = 32, K = 16, \text{and} N = 16$. Figure 2 depicts the relationship between the SE and the maximum transmit power of BS. It also highlights that for low values of $P_{\max}$, the problem is almost always infeasible. This outcome is anticipated as the BS lacks sufficient transmit power to fulfill the rate requirements of the users, resulting in very low SE values. However, when $P_{\max} \geq 16$ dBm, the achievable SE begins to increase. The turning point is a result of optimizing for EE rather than SE. When maximizing SE, the objective is to fully utilize all available BS power, leading to a continuously increasing trend in SE. However, maximizing EE involves finding the optimal balance between spectral efficiency and power consumption, which require increasing the BS transmit power beyond a threshold value. Due to the active structure of the AF relay, as opposed to the passive reflecting structure of the RIS, the AF relay exhibits the best performance, as shown in Fig. 2. However, as $P_{\max}$ increases, the performance gap between the RIS and AF relay becomes smaller, as the SE is dominated by BS transmit power.

The EE performance is shown in Fig. 3. The result confirms the non-monotonicity of EE versus $P_{\max}$ for all the schemes. When $P_{\max} \geq 25$ dBm, the excess transmit power is not used since it will decrease the energy efficiency. Also, the proposed algorithms for

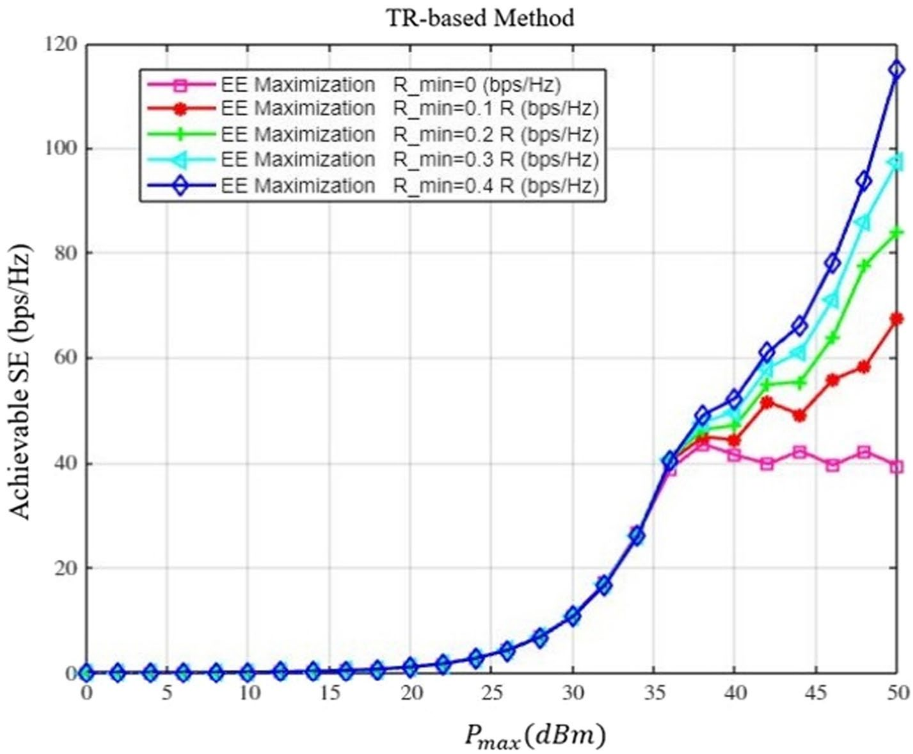

Fig. 4 Average SE using RIS versus $P_{\max}$ and $M = 32, K = 16, N = 16$ as well as different values for $R_{\min}$

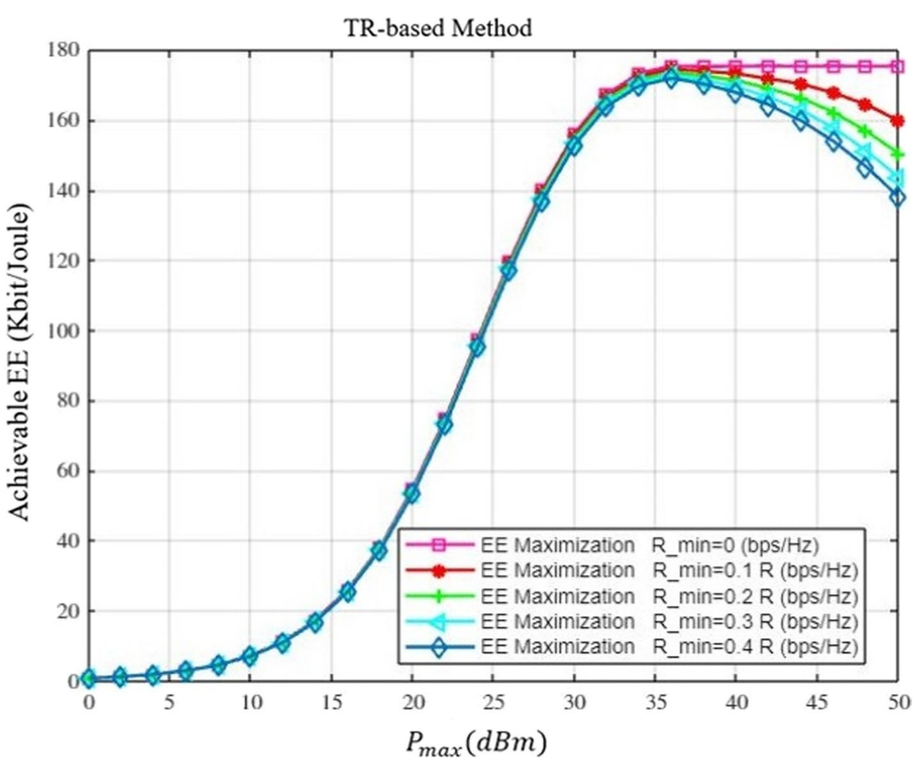

Fig. 5 Average EE using RIS versus $P_{\max}$ and $M = 32, K = 16, N = 16$ as well as different values for $R_{\min}$

the RIS-based system case significantly outperform the AF relay-assisted one in terms of EE, as the RIS is a passive terminal. Moreover, the performance of TR-based algorithm is better than other methods as can be observed in both Figs. 2 and 3.

The effect of the different values for $R_{\min}$ in the TR-based algorithm's SE and EE versus $P_{\max}$ in dBm is depicted in Figs. 4 and 5, respectively. All of the schemes' SE values are extremely low for small $P_{\max}$ values at BS, which cannot meet the consumers' minimum rate requirements. However, increasing $R_{\min}$ values results in increasing the achievable SE for $P_{\max} > 37$ dBm. Increasing $R_{\min}$ leads to higher achievable SE, outperforming the unconstrained case of $R_{\min} = 0$bps/Hz. A larger $R_{\min}$ value result in a steeper slope in the SE curve.The performance behavior in Fig. 5 follows the same trend as in Fig. 4. It is shown that for larger $P_{\max}$, higher values of $R_{\min}$ results in faster reduction of the EE, since the extra BS transmit power is used to satisfy the user rate requirements. Besides, the achieved EE versus number of RIS reflecting elements N for different methods is shown in Fig. 6. The figure shows that, as the number of RIS reflecting elements N increases, the EE performance of all schemes initially improves, but it eventually reaches a saturation point for $N > 12$ values and it predicted to have a decreasing trend for a very large number of N. Therefore, there is an optimal number of reflecting elements for EE maximization problem.

We also compared the performance of different algorithms in terms of EE and CPU run time. Figure 7 illustrates that the TR-based method achieves faster convergence towards a highly accurate optimal solution, leading to its superior EE performance.

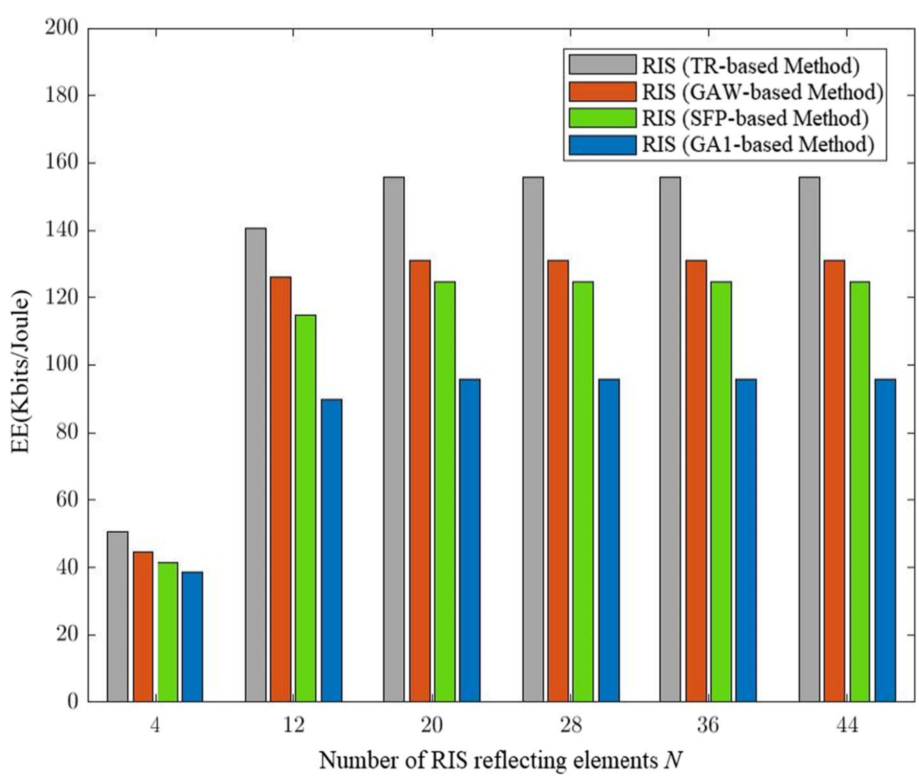

Fig. 6 EE using RIS versus N for SNR $= 20$dB and $R_{\min} = 0.2$ bps/Hz, as well as $P_n(b) = 0.01$dBm, $M = 64$, and $K = 16$

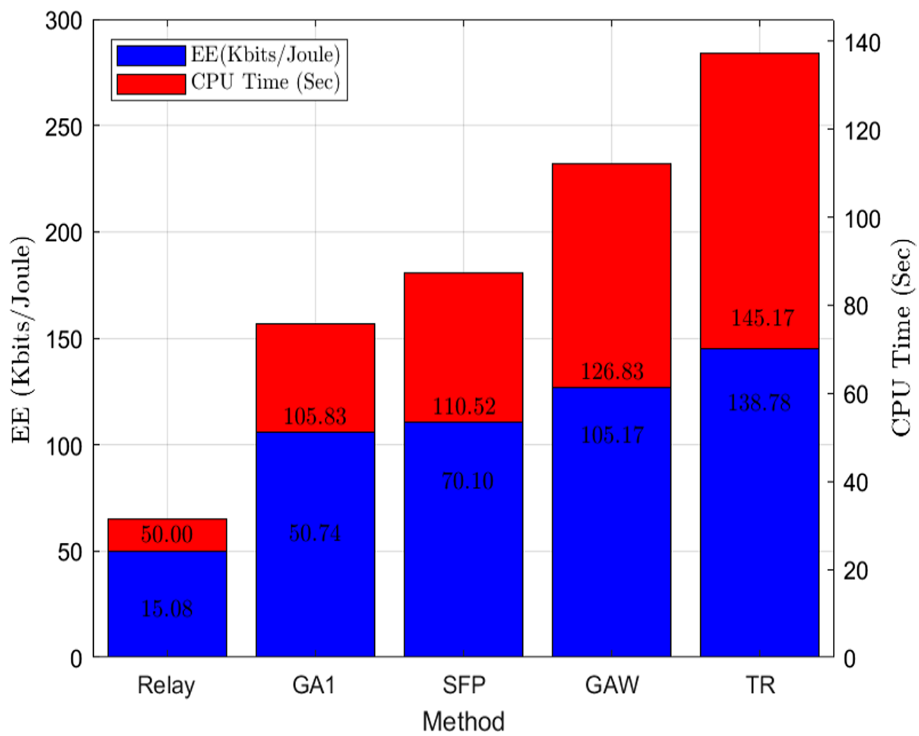

Fig. 7 EE and CPU time consumption of different algorithms for SNR $= 20$ dB and $R_{\min} = 0.2$ bps/Hz, as well as $P_n(b) = 0.01$ dBm, $M = 64$, and $K = N = 8$

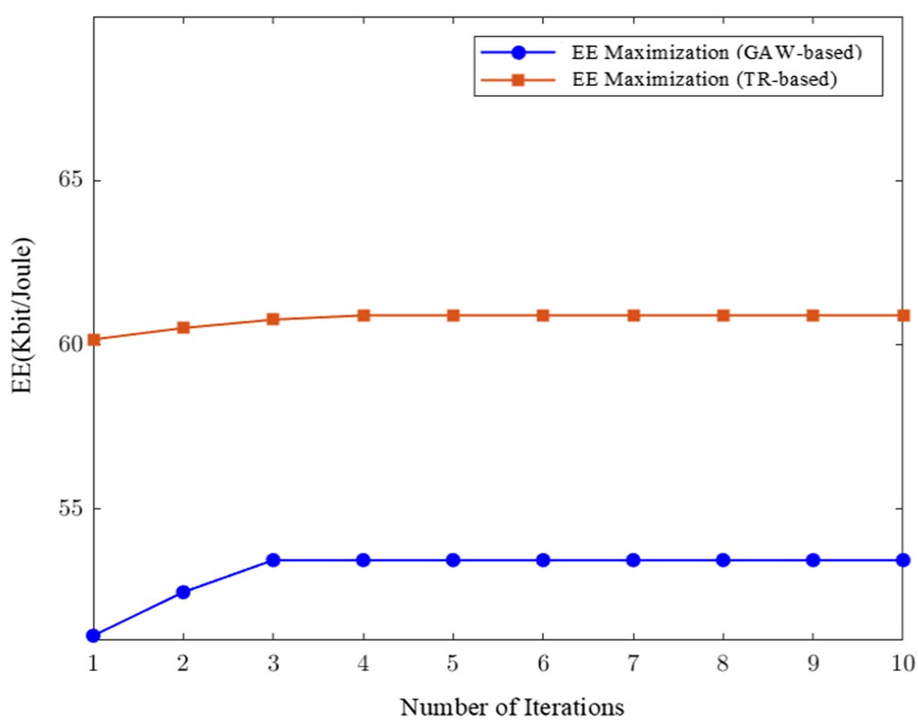

Fig. 8 EE versus number of iterations of different algorithms for SNR $= 20$ dB and $R_{\min} = 0.2$ bps/Hz, as well as $P_n(b) = 0.01$ dBm, $M = 64$, and $K = N = 8$

However, this advantage comes with the trade-off of requiring more CPU time compared to the other methods. Furthermore, Fig. 8 presents the convergence behaviors of the proposed methods. The EE is plotted against the number of iterations. The TR-based method demonstrates a faster convergence behavior compared to the GAW-based method. From the figure, it can be observed that the TR-based method converges rapidly in approximately one iteration. On the other hand, the GAW-based method takes more time to converge, reaching convergence after around three iterations.

4 CONCLUSION

In this paper, energy-efficient design and power allocation for RIS-based MISO networks in the downlink direction is investigated. After the introduction and formulation of the problem, RIS phase design and power allocation using TR- and GAW-based EE maximization methods are presented. Then, simulation results are compared with those of GA-based and SFP-based method and also a conventional method using the relay. Results show that TR- and GAW-based EE maximization method has improved energy efficiency in comparison to these methods.

This work primarily focuses on AO-based approaches for energy-efficient RIS-assisted MISO systems, leveraging the benefits of model-based optimization. However, we acknowledge the potential of ML techniques to further enhance our solutions by exploiting their adaptive capabilities and ability to capture complex system behaviors. Future work will explore advanced ML techniques and consider their integration with model-based algorithms to maximize the energy efficiency of RIS-aided wireless networks.

Abbreviations

UE	User
RF	Radio frequency
EE	Energy efficiency
SE	Spectral efficiency
RB	Resource block
GA	Gradient decent algorithm
QoS	Quality of Service
ZF	Zero-forcing
RIS	Reconfigurable intelligent surface
OFDM	Orthogonal frequency division multiplexing
OFDMA	Orthogonal frequency division multiple access
SISO	Single input single output
MISO	Multiple input single output
MIMO	Multiple input multiple output
APs	Access points
MU	Multiple user
SNR	Signal to noise ratio
AWGN	Additive white gussian noise
CSI	Channel state information
MC	Monte Carlo
AO	Alternating optimization
GA	Gradient-descent algorithm
GAW	Gradient-descent algorithm using Wolf conditions
TR	Trust Region
SCA	Successive convex approximation
FP	Fractional programming
BnB	Branch-and-bound
ML	Machine learning

Acknowledgements
The authors wish to convey their appreciation to every anonymous reviewer for their priceless feedback.

Author Contributions
SB conceived and designed the study, performed the simulations, and wrote the paper. MAO and MB have reviewed and discussed the technical details. All authors made suggestions for the improvements of the paper. All authors read, revised and approved the manuscript. SB and MAO oversaw the entire paper submission process. All authors read and approved the final manuscript.

Funding
This study received no external funding.

Availability of data and materials
Please contact the corresponding author at samaneh.bidabadi@uqtr.ca.

Declarations

Competing interests
The authors declare that they have no competing interests.

Received: 29 March 2023 Accepted: 22 August 2023
Published online: 05 September 2023

References

1. N. Rajatheva, I. Atzeni, E. Bjornson, A. Bourdoux, S. Buzzi, J.B. Dore, S. Erkucuk, M. Fuentes, K. Guan, Y. Hu, X. Huang, White paper on broadband connectivity in 6G. arXiv preprint arXiv:2004.14247. (2020)
2. W. Saad, M. Bennis, M. Chen, A vision of 6G wireless systems: applications, trends, technologies, and open research problems. IEEE Netw. **34**(3), 134–42 (2019)
3. Mitra P, Bhattacharjee R, Chatterjee T, De S, Karmakar R, Ghosh A, Adhikari T. Towards 6G Communications: Architecture, Challenges, and Future Directions. In2021 12th International Conference on Computing Communication and Networking Technologies (ICCCNT) 2021 Jul 6 (pp. 1–7). IEEE.
4. C. Huang, A. Zappone, G.C. Alexandropoulos, M. Debbah, C. Yuen, Reconfigurable intelligent surfaces for energy efficiency in wireless communication. IEEE Trans. Wirel. Commun. **18**(8), 4157–70 (2019)
5. Z. Yang, M. Chen, W. Saad, W. Xu, M. Shikh-Bahaei, H.V. Poor, S. Cui, Energy-efficient wireless communications with distributed reconfigurable intelligent surfaces. IEEE Trans. Wirel. Commun. **21**(1), 665–79 (2021)
6. H. Zhou, M. Erol-Kantarci, Y. Liu, H.V. Poor, A Survey on Model-based, Heuristic, and Machine Learning Optimization Approaches in RIS-aided Wireless Networks. arXiv preprint arXiv:2303.14320. (2023)
7. Q. Wu, G.Y. Li, W. Chen, D.W. Ng, R. Schober, An overview of sustainable green 5G networks. IEEE Wirel. Commun. **24**(4), 72–80 (2017)
8. B. Feng, J. Gao, Y. Wu, W. Zhang, X.G. Xia, C. Xiao, Optimization techniques in reconfigurable intelligent surface aided networks. IEEE Wirel. Commun. **28**(6), 87–93 (2021)
9. C. Huang, A. Zappone, M. Debbah, C. Yuen, Achievable rate maximization by passive intelligent mirrors. In 2018 IEEE International Conference on Acoustics, Speech and Signal Processing (ICASSP) (pp. 3714–3718). IEEE (2018)
10. Q. Wu, R. Zhang, Intelligent reflecting surface enhanced wireless network via joint active and passive beamforming. IEEE Trans. Wirel. Commun. **18**(11), 5394–409 (2019)
11. Y. Yang, S. Zhang, R. Zhang, IRS-enhanced OFDM: Power allocation and passive array optimization. In 2019 IEEE Global Communications Conference (GLOBECOM) (pp. 1–6). IEEE (2019)
12. P. Wang, J. Fang, X. Yuan, Z. Chen, H. Li, Intelligent reflecting surface-assisted millimeter wave communications: joint active and passive precoding design. IEEE Trans. Veh. Technol. **69**(12), 14960–73 (2020)
13. Y. Yang, B. Zheng, S. Zhang, R. Zhang, Intelligent reflecting surface meets OFDM: protocol design and rate maximization. IEEE Trans. Commun. **68**(7), 4522–35 (2020)
14. Y. Yang, S. Zhang, R. Zhang, IRS-enhanced OFDMA: joint resource allocation and passive beamforming optimization. IEEE Wirel. Commun. Lett. **9**(6), 760–4 (2020)
15. Q. Wu, R. Zhang, Intelligent reflecting surface enhanced wireless network via joint active and passive beamforming. IEEE Trans. Wirel. Commun. **18**(11), 5394–409 (2019)
16. Q. Wu, R. Zhang, Beamforming optimization for intelligent reflecting surface with discrete phase shifts. In ICASSP 2019-2019 IEEE International Conference on Acoustics, Speech and Signal Processing (ICASSP) (pp. 7830–7833). IEEE (2019)
17. F. Tan, X. Xu, H. Chen, S. Li, Energy-efficient beamforming optimization for MISO communication based on reconfigurable intelligent surface. Phys. Commun. **3**, 101996 (2023)
18. Z. Yang, M. Chen, W. Saad, W. Xu, M. Shikh-Bahaei, H.V. Poor, S. Cui, Energy-efficient wireless communications with distributed reconfigurable intelligent surfaces. IEEE Trans. Wireless Commun. **21**, 665–679 (2021)
19. O. Ozdogan, E. Bjornson, Deep learning-based phase reconfiguration for intelligent reflecting surfaces. In: Proceedings of Asilomar Conference on Signals, Systems, and Computers, pp. 707–711 (2020)
20. G. Lee, M. Jung, A.T.Z. Kasgari, W. Saad, M. Bennis, Deep reinforcement learning for energy-efficient networking with reconfigurable intelligent surfaces. In: Proceeings of IEEE International Conference on Communications (ICC), pp. 1–6 (2020)

21. X. Liu, Y. Liu, Y. Chen, H.V. Poor, RIS enhanced massive non-orthogonal multiple access networks: deployment and passive beamforming design. IEEE J. Sel. Areas Commun. **39**(4), 1057–1071 (2020)
22. S. Wright, J. Nocedal, Numerical optimization. Science. **35**(67–68), 7 (1999)
23. A. Zappone, L. Sanguinetti, G. Bacci, E. Jorswieck, M. Debbah, Energy-efficient power control: a look at 5G wireless technologies. IEEE Trans. Signal Process. **64**(7), 1668–83 (2015)
24. Zappone A, Jorswieck E, Energy efficiency in wireless networks via fractional programming theory. Found. Trends® Commun. Inform. Theory. **11**(3-4), 185–396 (2015)
25. A. Magbool, V. Kumar, M.F. Flanaga, On Energy Efficiency and Fairness Maximization in RIS-Assisted MU-MISO mmWave Communications. arXiv preprint arXiv:2211.08224. (2022)
26. P. Guan, Y. Wang, H. Yu, Y. Zhao, Energy efficiency maximisation for STAR–RIS assisted full–duplex communications. IET Commun. (2023)
27. V. Nesterov, How to make the gradients small. OPTIMA MPS Newslett. **88**, 10–11 (2012)
28. J.C. Gilbert, J. Nocedal, Global convergence properties of conjugate gradient methods for optimization. SIAM J. Optim. **2**(1), 21–42 (1992)
29. K. Ritter, On the rate of superlinear convergence of a class of variable metric methods. Numerische Mathematik **35**, 293–313 (1980)
30. S. Gratton, A. Sartenaer, P.L. Toint, Recursive trust-region methods for multiscale nonlinear optimization. SIAM J. Optim. **19**, 414–444 (2008)
31. Y.X. Yuan, Recent advances in trust region algorithms. Math. Program. **151**, 249–81 (2015)
32. E. Björnson, L. Sanguinetti, J. Hoydis, M. Debbah, Optimal design of energy-efficient multi-user MIMO systems: is massive MIMO the answer? IEEE Trans. Wirel. Commun. **14**(6), 3059–75 (2015)

Publisher's Note

Springer Nature remains neutral with regard to jurisdictional claims in published maps and institutional affiliations.